HHS Public Access

Author manuscript

Dev Cell. Author manuscript; available in PMC 2021 October 26.

Published in final edited form as:

Dev Cell. 2020 October 26; 55(2): 224–236.e6. doi:10.1016/j.devcel.2020.09.016.

Super-resolution Microscopy and FIB-SEM Imaging Reveal Parental Centriole-Derived, Hybrid Cilium in Mammalian Multiciliated Cells

Zhen Liu[1,2,11], **Quynh P.H. Nguyen**[1,2,11], **Rashmi Nanjundappa**[3], **Nathalie Delgehyr**[4], **Alexandre Megherbi**[4], **Regan Doherty**[5], **James Thompson**[6], **Claire Jackson**[6], **Alexandra Albulescu**[2], **Yew Heng**[7], **Jane S Lucas**[6], **Sharon D. Dell**[8], **Alice Meunier**[4], **Kirk Czymmek**[9], **Moe R. Mahjoub**[3,10], **Vito Mennella**[1,2,6,12,*]

[1]Biochemistry Department, University of Toronto, Toronto, ON M5S1A8, Canada.

[2]Cell Biology Program, The Hospital for Sick Children, Toronto, ON M5G0A4, Canada.

[3]Department of Medicine, Nephrology Division, Washington University, St Louis, MO 63310, USA

[4]Cilia biology and neurogenesis, Institut de biologie de l'Ecole normale supérieure (IBENS), CNRS, INSERM, PSL Université, Paris, 75005, France.

[5]Biomedical Imaging Unit, Faculty of Medicine, University of Southampton, Southampton, SO16 6YD, UK

[6]NIHR Southampton Biomedical Research Center, Clinical & Experimental Sciences, Faculty of Medicine, University of Southampton, Southampton, SO16 6YD, UK

[7]Paediatric Laboratory Medicine (PLM), The Hospital for Sick Children, Toronto, ON M5G1X8, Canada.

[8]Child Health Evaluative Sciences, Program, The Hospital for Sick Children, Toronto, ON M5G0A4, Canada.

[9]Carl Zeiss Microscopy, Thornwood, NY 10601, USA.

[10]Department of Cell Biology and Physiology, Washington University, St Louis, MO 63310, USA

[12]Lead contact

[*]Correspondence: v.mennella@soton.ac.uk.

[11]These authors contributed equally

AUTHOR CONTRIBUTIONS

Z.L. and Q.P.H.N. conducted experiments, collected and analysed the data, wrote methods and edited the manuscript. A.A. helped with airway multiciliated cells culturing system; R.N. performed the mouse tracheal epithelia cell experiments; J.T. performed *ex vivo* trachea labelling experiments; C.J. helped with trachea labelling and edited the manuscript; R.D. and Y.H. performed TEM on CCNO PCD patients; M.M. and V.M. conceived and designed the MTEC-centrinone experiments; N.D., M.A and A.M. conceived and performed the ependymal cells pulse chase experiments; S.D. and J.S.L provided PCD patients cells, K.C. helped with sample preparation for FIB-SEM data collection and acquired data; V.M. conceived the project, designed experiments, analysed data and wrote the manuscript.

DECLARATIONS OF INTERESTS

The authors declare no competing financial interests.

SUMMARY

Motile cilia are cellular beating machines that play a critical role in mucociliary clearance, cerebrospinal fluid movement and fertility. In the airways, the hundreds of motile cilia present on the surface of a multiciliated epithelia cell beat coordinately to protect the epithelium from bacteria, viruses and harmful particulates. During multiciliated cell differentiation, motile cilia are templated from basal bodies each extending a basal foot, an appendage linking motile cilia together to ensure coordinated beating. Here, we demonstrate that among the many motile cilia of a multiciliated cell, a hybrid cilium with structural features of both primary and motile cilia is harboured. The hybrid cilium is conserved in mammalian multiciliated cells, originates from parental centrioles and its cellular position is biased and dependent on ciliary beating. We further show that the hybrid cilium emerges independently of other motile cilia, and functions in regulating basal body alignment.

Graphical Abstract

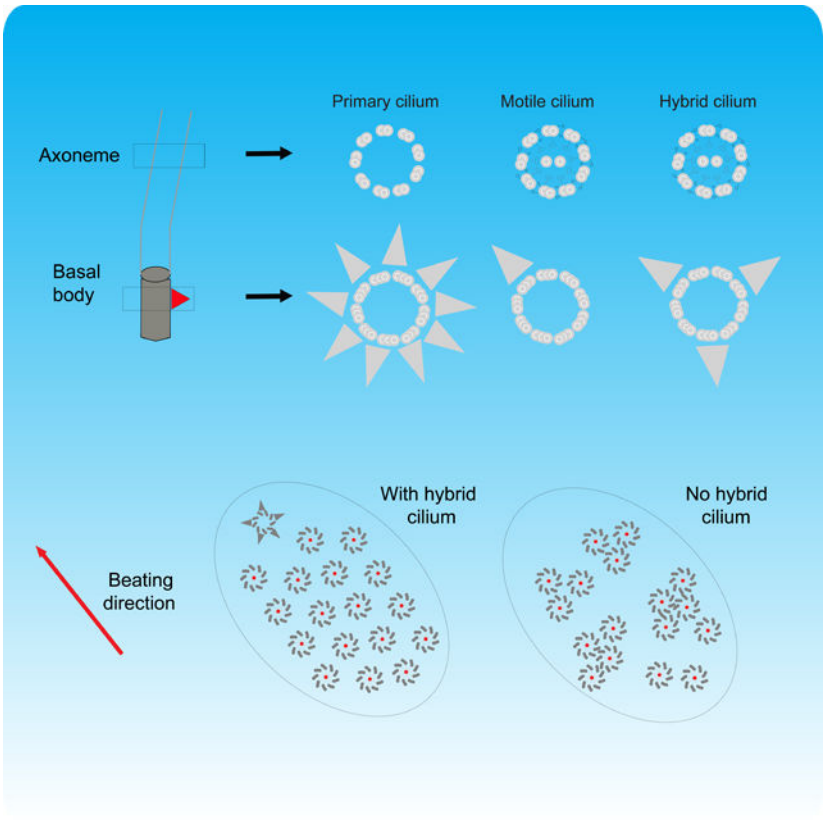

eTOC:

Liu, Nguyen et al. show that among hundreds of cilia of a multiciliated cell, there is one that differs from the others in structure, origin and cellular position, which participates in basal body alignment.

INTRODUCTION

Motile cilia are beating organelles found on the surface of specialized epithelial cells that generate the propulsive force required for critical physiological activities such as mucociliary clearance, ependymal cerebrospinal fluid circulation and ovum directional movement in the fallopian tubes (Reiter and Leroux, 2017; Spassky and Meunier, 2017). In the airways, the hundreds of motile cilia within one multiciliated cell beat cooperatively to remove bacteria, viral particles and environmental pollutants, thereby helping the immune system clearing infections and ensuring lung health (Lucas et al., 2020; Reiter and Leroux, 2017).

To beat in coordination, motile cilia rely on the basal foot, a conical structure attached to the basal body on one end, and to the microtubule cytoskeleton on the other, thereby linking motile cilia together in a network (Clare et al., 2014; Kunimoto et al., 2012; Vladar et al., 2012). The hundreds of motile cilia on the surface of a multiciliated cell are thought to be identical to one another (Jain et al., 2010; Spassky and Meunier, 2017), templated from basal bodies each with one basal foot. When motile cilia beat coordinatively, basal bodies are aligned in rows with their basal feet pointing toward the direction of ciliary beating (Boisvieux-Ulrich et al., 1985; Frisch and Farbman, 1968; Gibbons, 1961), a phenomenon termed rotational polarity (Marshall and Kintner, 2008; Mitchell et al., 2007).

In airway cells, loss of basal feet results in disorganization of the microtubule apical network, irreversible disorientation of basal bodies and loss of motile cilia coordination (Herawati et al., 2016). In mice (Kunimoto et al., 2012), this leads to respiratory manifestations consistent with primary ciliary dyskinesia (PCD), a human rare disease characterized by chronic airway infections, bronchiectasis and frequently associated with conductive hearing loss, male infertility, heterotaxy and cardiac malformations (Kunimoto et al., 2012; Lucas et al., 2020).

In addition to multiciliated cells, the basal foot is also present in cells protruding a primary cilium. Its suggested function is to keep the primary cilium submerged in certain cell types by linking the basal body to Golgi, in concert with the pool of centrosomal proximal end proteins. In turn this controls ectopic Shh-signalling activation (Galati et al., 2016; Mazo et al., 2016). Different from motile cilia, the basal foot of the primary cilium has multiple copies per basal body and it is thought to originate from nine (or less depending on the cell type) subdistal appendages, mother centriole-associated structures contributing to the organization of the interphase microtubule array (Chong et al., 2020; Paintrand et al., 1992; Uzbekov and Alieva, 2018).

We have recently resolved the molecular architecture of the basal foot *in situ* by super-resolution microscopy in primary and motile cilia (Nguyen et al., this issue). In the process of determining the molecular map of basal foot in motile cilia, we discovered the presence of a “hybrid” cilium in multiciliated cells. This hybrid cilium is characterized by a basal body containing multiple basal feet, resembling a primary cilium, but expressing proteins and with an axonemal ultrastructure typical of motile cilia. Here we characterize hybrid cilium structure, conservation, formation and function in airway multiciliated cells.

RESULTS

Identification of a Hybrid Cilium in Airway Multiciliated Cells

Previous studies have indicated that the basal foot shows both structural and numerical differences in the two ciliary systems: the most obvious one is that primary cilia have multiple basal feet per basal body, while motile cilia have one basal foot per basal body (Boisvieux-Ulrich et al., 1985; Frisch and Farbman, 1968; Gibbons, 1961; Kunimoto et al., 2012; Mitchell et al., 2007). While imaging basal foot proteins in human airway multiciliated cells, it was therefore surprising to observe a ring-like pattern of basal foot proteins in addition to the expected dot pattern for a single basal foot (Figures 1A, 1B and 1C, see boxed regions). This arrangement suggested the presence of a basal body in a multiciliated cell similar to that of a primary cilium (Figure 1B).

To validate this initial observation, we collected micrographs of primary nasal human multiciliated cells grown in an air-liquid interface co-labelled with antibodies recognizing different basal foot (CNTRL, CEP128) and basal body (POC1B) proteins by 3D structured illumination microscopy (3D-SIM) (Figures 1B and S1). This analysis demonstrated that the ring pattern resulted from a single basal body with multiple basal feet, and not from multiple basal bodies clustering together as in the compound cilium, a membrane-delimited structure made of multiple motile cilia clustered together, which is frequently found in airway cells after injury (McAuley and Anand, 1998).

Imaging of freshly isolated nasal epithelial human cells established that this basal body is also present in tissue *ex vivo* and not only in primary cell culture systems (Figure 2A). To confirm its presence by other imaging methods, we used stochastic optical resolution fluorescence microscopy (STORM), a technique reaching routinely ~25 nm in plane resolution, as well as transmission electron microscopy (TEM) to examine sections of airway cells differentiated *in vitro.* Both imaging methods confirmed the presence of this basal body (Figures 2B and 2C). TEM and 3D-SIM also showed that it templates a cilium (Figures 2D and 2E).

To assess the conservation of the hybrid cilium beyond airway epithelium, multiciliated cells differentiated from mouse tracheal and brain ependymal tissue progenitors were examined. Using 3D-SIM, a basal body associated with multiple basal feet was observed in each cell type, showing that the hybrid cilium is an organelle present in multiple tissues that have multiciliated cells, both in mouse and human (Figures 2F and 2G).

The Cilium Discovered has Features of Primary and Motile Cilia

Next, we asked which type of cilium was templated from this basal body with multiple basal feet. To address this question, we examined its ultrastructure by Focused Ion Beam-Scanning Electron Microscopy (FIB-SEM), an EM technique capable of imaging large volumes, several cells wide, with isotropic resolution (Figure 3A) (Kizilyaprak et al., 2019). Analysis of tomographic sections confirmed that this basal body templates a *bona fide* cilium (consistent with Figures 2D and 2E) and showed that it contains a central pair of microtubules (a structure required for in plane beating) as the surrounding motile cilia in the same multiciliated cell (Figures 3B and 3C and Videos S1 and S2). 3D-SIM micrographs of

airway multiciliated cells labeled with anti-radial spoke head (RSPH4A) (Frommer et al., 2015) and nexin-dynein regulatory complex (GAS8) (Olbrich et al., 2015) antibodies further demonstrated that this cilium harbours components of the ciliary beating machinery (Figure 3D).

Altogether, our data show that in human airway multiciliated cells, not all the cilia are identical, and that a single cilium presents hybrid features of both primary and motile cilia, namely multiple basal feet and proteins associated with the ciliary beating machinery (Figure 3E).

The Hybrid Cilium Originates from Parental Centrioles

A long-standing question in the field of multiciliated cell development has been the fate of parental centrioles after multiciliogenesis, which are initially present in precursor basal stem cell as a mother-daughter engaged pair in the centrosome (Jain et al., 2010). The presence of multiple basal feet typical of primary cilia suggested the possibility that the hybrid cilium originates from the mother centriole, which in mouse airway multiciliated cells first templates the primary cilium present during the early stages of differentiation (Jain et al., 2010), then is resorbed before centriole amplification through the canonical and deuterosome pathway (Al Jord et al., 2014; Vladar and Stearns, 2007; Zhao et al., 2013).

To first test whether the mother and daughter centrosomal centrioles are retained in differentiated multiciliated cells, we performed a pulse-chase experiment allowing to label differentially centrosomal centrioles from newly formed basal bodies in mouse cultured ependymal cells (Figure S2). Time-lapse monitoring of RFP-Cen1 centrosomal centrioles in cells from transgenic mice expressing Cen2-EGFP, which labeled newly formed basal bodies (Higginbotham et al., 2004) showed that centrosomal centrioles are retained within the newly formed basal body patch and are capable of growing cilia (Figure S2, Video S3). However, we could not confirm whether the centrosomal centrioles present multiple basal feet by 3D-SIM due to the low number of cells with centrioles expressing both RFP-Cen1 and Cen2-GFP and their oblique orientation at the surface of ependymal cells differently from airway cells.

To further test our hypothesis that the hybrid cilium is derived from the mother centriole, we then used centrinone A, a small molecule drug blocking canonical centriole duplication by inhibiting Plk4, a kinase critical for the early stages of centriole duplication, to deplete cells of parental centrioles (Figure 4A) (Wong et al., 2015). As expected, basal cells isolated from mouse trachea treated with centrinone A showed a reduction in centrioles before airway cell differentiation (Figure S3) (Nanjundappa et al., 2019). When cells were treated with centrinone A either only during basal cell expansion or also throughout differentiation of mouse trachea airway cells (MTEC), drug treatment did not impact multiciliated cell formation (Figure S3), as previously described (Nanjundappa et al., 2019). However, centrinone A treatment caused a reduction in hybrid cilia number in the mature multiciliated cell stage, indicating that the hybrid cilium originates from parental centrioles, most likely the mother that initially harbours subdistal appendages/basal feet (Figures 4B, 4C and 4D).

Hybrid Cilium Formation is Independent from Other Motile cilia

Despite sharing the same cellular environment during differentiation, the hybrid cilium origin and structure are different from all other motile cilia. This suggested the possibility that hybrid cilium formation is determined independently of other motile cilia in the same multiciliated cell.

Interestingly, previous studies have established that mutations in certain human disease genes causing PCD are characterized by a lack, or a diminished number, of motile cilia. This phenotype, named oligocilia or reduced generation of multiple cilia (RGMC) is determined by loss-of-function mutations in PCD genes (Lucas et al., 2020) encoding transcription factors and regulators of the multiciliogenesis program such as the nuclear protein MCIDAS (Boon et al., 2014; Stubbs et al., 2012), the transcription factor FOXJ1 (Gomperts et al., 2004; Wallmeier et al., 2019) and the transcriptional regulator CCNO (Funk et al., 2015; Wallmeier et al., 2014) (Figure 5A). In particular, multiciliated cells isolated from patients with mutations in *CCNO* present on their surface mainly one cilium per cell, occasionally two or sparse cilia ((Wallmeier et al., 2014) and our observations). *MCIDAS* loss-of-function patient and KO mice cells can also present one basal body/cilium per cell, albeit less frequently than in *CCNO* mutations (Boon et al., 2014; Lu et al., 2019). In the case of *CCNO* mutant cells, this solitary cilium beats, indicating that it has acquired motility machinery (Wallmeier et al., 2014).

To test the hypothesis that the hybrid cilium is in fact the single cilium reaching the surface of multiciliated cells in oligocilia/RGMC patients, we recruited two individuals with different loss-of-function mutations in *CCNO* and analysed their cells extensively using TEM sections. Our data clearly showed that cells from PCD patients with rare *CCNO* mutations present a cilium with multiple basal feet per basal body as in the hybrid cilium (Figure 5B).

Altogether, our data show that the hybrid cilium and “CCNO cilium” share the same structure, thereby suggesting that hybrid cilium formation is determined even in the absence of other motile cilia on the surface of airway multiciliated cells.

Hybrid Cilium Position is Biased Toward the Direction of Beating and Functions in Basal Body Alignment

It has previously been shown that during multiciliated cell differentiation, motile cilia first generate fluid flow, then fine-tune their position within a cell to generate a more effective directional flow and mucociliary transport (Guirao et al., 2010; Mitchell et al., 2007). Since an established basal foot function in multiciliated cells is to link basal bodies together through microtubule cables (Kunimoto et al., 2012), we hypothesized that the hybrid cilium could function to align basal bodies in the direction of flow.

To test this hypothesis, we first evaluated its relative position in cells. We developed a MATLAB image analysis script locating the position of the hybrid cilium relative to beating direction, which was measured by basal body-basal foot rotational polarity in multiciliated cells (Figure 6A). This analysis confirmed quantitatively that the hybrid cilium is positioned preferentially in the front end relative to the beating direction as suggested by our 3D-SIM

images (Figure 6B, see also Figure 1A). To establish whether this positional bias was dependent on ciliary beating, we analysed cells from three PCD patients with independent loss of function mutations in outer dynein arm proteins (two patients with mutations in DNAH5 (PCD 1 and PCD 3) and one with DNAH11 (PCD 2), (Key Resource Table); both proteins are critical for ciliary motility, but their loss of function does not impact basal body formation (Knowles et al., 2012; Omran et al., 2000)). As expected, PCD patients' cells exhibited normal ciliation, impaired ciliary beating and reduced rotational polarity (Figure S4) (Knowles et al., 2012; Liu et al., 2020; Omran et al., 2000). Notably, the hybrid cilium from PCD patient cells was found to be more "centred" in the cell (Figures 6B and S4), similar to the position of centrosomes in cycling cells. To further confirm the "biased" location of the hybrid cilium within a multiciliated cell, we assessed its position relative to the cell centroid and membrane, irrespective of motile cilia beating direction. Consistent with our previous analysis, the hybrid cilium in cells from PCD patients was located closer to the cell centre than in healthy controls (Figures 6C and S4).

Finally, we sought to determine whether directional flow generated during multiciliated cell differentiation helps to position the hybrid cilium. In order to mimic conditions in the airway, mouse tracheal progenitor cells were subjected to mechanical agitation to induce directional surface flow during their differentiation, thereby promoting basal body and cellular alignment (Guirao et al., 2010). Indeed, analyses of mouse tracheal cells confirmed that the hybrid cilium becomes positioned in the front end of the cells toward the direction of flow (Figure 6D), consistent with what was observed in human primary cultures (Figures 1A and 6B) and mouse tracheal tissue explant (Figure 6E). Altogether these data show that the hybrid cilium position is biased towards the direction of beating and that its position is influenced by external flow and ciliary motility.

Interestingly, labelling of mouse trachea with microtubule nucleating and anchoring complex protein γ-Tubulin showed that multiple basal feet of the hybrid cilium are competent for linkage to the microtubules network (Figures 6E and 6F). To better understand the function of the hybrid cilium, mouse tracheal cells were then treated with centrinone A to inhibit hybrid cilia formation, and cells were subjected to directional flow as described above. The chemical approach was the only available method for loss of function studies, since hybrid cilium protein composition is not yet known and therefore no targets for selective genetic removal during ciliogenesis are available. To ensure maximal hybrid cilia reduction, centrinone A was used throughout mouse tracheal airway multiciliated cell differentiation, a treatment that did not impact multiciliated cell formation (Nanjundappa et al., 2019). As previously observed, airway cells in both DMSO and centrinone A-treated conditions showed similar ciliation levels and overall comparable tissue level organization, with some noticeable differences in cellular alignment (Nanjundappa et al., 2019) (Figures 7A–7D). However, while cells treated with vehicle control showed basal bodies locally aligned in rows as expected (Figures 7A and 7B), cells depleted of the hybrid cilium show impaired basal body alignment as evidenced by the staining of basal body component CEP135 (Figures 7C and 7D).

To quantify the changes in basal body organization, the positions of basal bodies within each cell were analysed for local alignment and then averaged to a global alignment index for

each cell with custom MATLAB scripts, similar to previously described methods (Herawati et al., 2016). This quantitative analysis demonstrates that hybrid cilium depletion leads to a significant reduction in alignment index for the multiciliated cells (mean=0.23±0.09 as compared to 0.33±0.05, n=63 (DMSO); n=70 cells (Centrinone A)), suggesting an overall basal body organization disruption at the cellular level (Figures 7B, 7D and 7E). Altogether, our data show that the hybrid cilium regulates basal body alignment in multiciliated cells (Figure 7F).

DISCUSSION

Our study led to the surprising discovery that a different cilium is harboured among the hundreds of motile cilia in a differentiated multiciliated cell. The hybrid cilium has features of motile and primary cilia, including multiple basal feet as found in primary cilia, and a central pair apparatus and proteins required for ciliary beating as in motile cilia. Airway cells lacking hybrid cilium differentiate normally, extrude motile cilia, but lack effective basal body alignment.

Our data reveal the fate of mother centriole in mature multiciliated cells, a major unanswered question in this field. In airway cells, during the early stages of differentiation - before Foxj1 expression - the mother centriole templates a primary cilium that is subsequently resorbed before centriole amplification (Jain et al., 2010). After this step, its role has remained mysterious. Here, we show that one of the parental centrioles, likely the mother, resurfaces to generate the hybrid cilium harboured among motile cilia. In agreement with results in airway cells, pulse-chase experiments in mouse cultured ependymal cells showed that centrosomal centrioles are retained within the newly formed basal body patch and are capable of growing cilia.

In airway cells differentiated *in vitro*, we observed a subpopulation of cells with two hybrid cilia, but less frequently so in *ex vivo* trachea and primary nasal airway cells. Our data suggest that mother centriole is the origin of the hybrid cilium, however we cannot rule out that a disengaged daughter centriole might reach the surface of multiciliated cells and express multiple basal feet. An alternative possibility is that basal stem cell duplication driven *in vitro* during population expansion might lead to an increase in cells with two mother centrioles due to mitotic division defects.

Notably, analysis of PCD patients with CCNO mutations leading to oligocilia demonstrates that hybrid cilium formation is determined independently of other motile cilia in the same multiciliated cell. This suggests two possible scenarios at play during multiciliated cells differentiation: one possibility is that CCNO patients' cells have lost the capacity to duplicate basal bodies of motile cilia, but are capable of executing the rest of the motile cilia formation program (including transport, docking and extension at the membrane). Supporting this view are previous studies from the Kintner lab in Xenopus that showed that RNA misexpression of FOXJ1 on surface epithelial cells, in a mutant background inhibiting motile cilia formation, leads to the emergence of a single cilium or biciliated cells on the surface of epithelia. These cilia exhibit a 9+2 axonemal microtubule structure, beat both in a rotational and in plane pattern and are of intermediate length between a primary and motile

cilia (Stubbs et al., 2008). Interestingly, though, these cilia of intermediate length do not seem to be present in mature human airway multiciliated cells (our observations). Alternatively, it is possible that a specific molecular program exists that is responsible for hybrid cilium formation, which is separate (at least in part), whose drivers and components remain unknown.

Interestingly, PCD patients with oligocilia mutations appear to have worse clinical outcomes than patients with mutations in most of the PCD genes leading to ciliary immotility (Boon et al., 2014; Wallmeier et al., 2014; Wallmeier et al., 2019). This suggests that additional molecular functions, beyond simply ciliary motility, might contribute to the poor clinical outcome.

The hybrid cilium is found to be preferentially positioned towards the direction of ciliary beating. Since effective flow generated by beating motile cilia is required to maintain the position of the hybrid cilium, this suggests that it responds to flow either directly or indirectly. The biased position of the hybrid cilium is reminiscent to that of the primary cilium at the leading edge in the wound region in vascular and bronchial smooth muscle cells, where it is thought to sense extracellular matrix proteins and promote cell migration (Lu et al., 2008; Wu et al., 2009). This biased position also resembles that of primary cilium in radial glia cells, the progenitors of ependymal cells, where it has been shown to regulate translational polarity - a basal body organization specific to ependymal multiciliated cells that is not found in the airway (Mirzadeh et al., 2010).

Our data show that loss of hybrid cilium by centrinone A treatment leads to reduced basal body alignment in airway cells. An interesting mechanistic explanation is that the multiple basal feet of the hybrid cilium function to align the different rows of basal bodies as a rudder of a sailboat; PCP proteins might also be affected by hybrid cilium removal (Mitchell et al., 2009; Vladar et al., 2012).

Notably, basal feet of primary cilia have been previously linked to TGFbeta signalling (Clement et al., 2013; Monnich et al., 2018). It is therefore a possibility that the hybrid cilium might harbour a different complement of signalling molecules compared to motile cilia, which might help explain its specialized function. Our initial efforts to detect primary cilia-specific markers specifically enriched at the hybrid cilium did not produce any valuable insight. Future studies are needed to address whether the hybrid cilium, in addition to being a distinct organelle structurally and functionally, also has specific signalling capabilities.

STAR METHODS

RESOURCE AVAILABILITY

Lead Contract—Further information and request for resources and reagents should be directed to and will be fulfilled by the Lead Contract, Vito Mennella (v.mennella@soton.ac.uk)

Materials Availability—All unique/stable reagents generated in this study are available from the Lead Contact with a completed Materials Transfer Agreement

Data and Code Availability—The published article includes all datasets generated during this study. Code is available by the Google Drive link specified in method details.

EXPERIMENTAL MODEL AND SUBJECT DETAILS

Mouse primary cells—Mouse tracheal epithelia primary cells were acquired from the trachea of C57BL/6 mice at 2–4 months of age, following protocols that are compliant with guidelines of the Institutional Animal Care and Use Committee at Washington University and the National Institutes of Health. For ependymal cell culturing, mouse strain Cen2-GFP (CB6-Tg(CAG-EGFP/CETN2)3–4Jgg/J, The Jackson Laboratory) was used to obtain primary cells, according to the guidelines of the European Community and French Ministry of Agriculture, approved by the Ethic comity Charles Darwin (C2EA-05) and “Direction départementale de la protection des populations de Paris”, (Approval number Ce5/2012/107; APAFiS #9343).

Human primary cells—Healthy volunteers and PCD patients were recruited and airway primary cells were obtained following a protocol approved by Research Ethics Board(REB #1000054690) at the Hospital For Sick Children and adhering to local and national research and ethical approval (Southampton and South West Hampshire Research Ethics 07/Q1702/109). PCD1 is 16 years old female with DNAH5 mutations (c1432C>T&c11571–1G>A). PCD2 is 9 years old female with DNAH11 mutations (c12888T>A&c12365T>G). PCD3 is 12 years old female with DNAH5 mutations (DNAH5 c1901_1902delTC).

METHOD DETAILS

Immortalized and Primary Cell Culture—Human primary nasal airway cells from healthy volunteers and PCD patients were collected with using a cytology brush by a nurse, following a protocol approved by Research Ethics Board(REB #1000054690) at the Hospital For Sick Children and adhering to local and national research and ethical approval (Southampton and South West Hampshire Research Ethics 07/Q1702/109). Airway cells were then expanded in PneumaCult-Ex media, seeded on transwells (Corning HTS Transwell-96 and −24 permeable support; 0.4 μm pore size), and differentiated for at least 21 days following Stem Cell Technologies protocols using PneumaCult-Ex and PneumaCult-ALI media. The media were supplemented with vancomycin, tobramycin, gentamicin and antibiotic-antimycotic antibiotics.

Immunofluorescence and Antibodies—Human nasal and mouse tracheal multiciliated cells from ALI cultures were directly fixed on Transwell filters with either methanol (20 min at −20°C) or 4 % paraformaldehyde (PFA; 10 min at room temperature (RT)). For PFA fixation, cells were subsequently reduced with 0.1% Sodium Borohydride for 7 minutes, then permeabilized with 0.2% Triton X-100 for 25 minutes. Cells were blocked using 5% FBS-containing PBS, incubated with primary antibodies for either 1 hour (RT) or overnight (4°C), and then secondary antibodies conjugated with Alexa FluorAlexafluor −405, −488, −555 orand −647 nm (Thermo Fisher Scientific). When appropriate, cells were stained with directly labeled primary antibodies (prepared using APEX Antibody Labeling Kit, Thermo Fisher Scientific and Mix-n-Stain Antibody Labeling Kit, Sigma-Aldrich). For STORM imaging, Alexa647 conjugated F(ab’)2 fragments were used conjugated. Please refer to key

resources table for a list of antibodies used in this study. Trachea labeling was performed essentially as in (Vladar et al., 2015). Briefly, mouse was euthanized by CO_2 asphyxiation, douse with 70% ethanol and trachea was isolated. The trachea was placed on ice cold Ham's F12 +1% pen-strep. The lumen of the trachea was then exposed by cutting it open longitudinally along the dorsal surface using dissecting scissors. The trachea was then fixed by adding −20 °C methanol over the tissue for 10 min, blocked with 10% normal serum in PBST (pH 7.4 +10% Triton X-100), incubated with primary antibodies for 1 hour (RT) and then fluorescent dye conjugated secondary antibodies for 30 minutes (RT). A flat and rectangular area of the trachea was finally cut out and mounted for subsequent imaging.

Super-resolution Imaging—3D-SIM data was collected using ELYRA PS.1 (Carl Zeiss Microscopy) with a Plan-Apochromat 63x or 100x/1.4 Oil immersion objective lens with an additional 1.6x optovar. An Andor iXon 885 EMCCD camera was used to acquire images with 101 nm/pixel z-stack intervals over a 5–10 μm thickness. For each image field, grid excitation patterns were collected for five phases and three rotation angles (−75°; −15°, +45°). The raw data was reconstructed and channel aligned using SIM module of ZEN Black Software (version 8.1). STORM data was collected using PALM mode in ELYRA PS.1 (Carl Zeiss Microscopy) with a Plan-Apochromat 63x or 100x/1.4 Oil immersion objective lens with an additional 1.6x optovar. An Andor iXon 885 EMCCD camera was used to acquire images using TIRF mode. Lasers of wavelength 647 nm and 405 nm were used to activate the fluorophore. Raw data was reconstructed using PALM module of Zen Black Software (version 8.1), with the account for overlapping molecules. Reconstructed data was further processed for drift correction and binning using home-written MATLAB script (can be accessed via the following link: https://drive.google.com/open?id=11fuWn7kmZ-loCn79CKChJI5FeMme0fDU).

Transmission Electron Microscopy (TEM)—ALI filters of fully differentiated human nasal multiciliated cells were fixed in 2% glutaraldehyde in 0.1M sodium cacodylate buffer. Samples were rinsed in 0.1M sodium cacodylate buffer with 0.2M sucrose, post-fixed in 1% OsO_4 in 0.1M sodium cacodylate buffer, dehydrated in a graded ethanol series (70%, 90%, 3X 100%), infiltrated with propylene oxide, and embedded in Quetol-Spurr resin. Serial sections (90 nm-thickness) were cut on a Leica Ultracut ultramicrotome, stained with uranyl acetate and lead citrate, and imaged in a FEI Tecnai 20 TEM.

Focused Ion Beam Scanning Electron Microscopy (FIB-SEM)—ALI filters of fully differentiated human nasal multiciliated cells were fixed in 2.5% glutaraldehyde and 0.05% malachite green oxalate in 0.1M sodium cacodylate buffer, rinsed in 0.1M sodium cacodylate buffer, post-fixed in 0.8% potassium ferrocyanide and 1% OsO_4 in 0.1M sodium cacodylate buffer. The samples were treated with 1% tannic acid, stained with 0.5% uranyl acetate, followed by dehydration in a graded acetone series (25%, 50%, 75%, 95% and 100%), and embedded in resin. Resin formulation: 18.2% Araldite M (Sigma-Aldrich), 22.7% Epon 812 (Sigma-Aldrich), 54.5% Hardener DDSA (Sigma-Aldrich) and 4.5% DMP-30 (Sigma-Aldrich). FIB-SEM imaging for Sup. Movie 1,2 was performed as described below. Sample blocks for analysis by FIB-SEM were trimmed and mounted on a 45° pre-titled SEM stub and coated with a 4-nm layer of Pt to enhance electrical

conductivity. Milling of serial sections and imaging of block face after each *Z*-slice was carried out with the FEI Helios Nanolab 660 DualBeam using Auto Slice & View G3 ver 1.5.3 software (FEI Company, Hillsboro, OR USA). A block was first imaged to determine the orientation relationship between the block face of ion and electron beams. A protective carbon layer 50 μm long, 8 μm wide and 2 μm thick was deposited on the surface of the region of interest to protect the resin volume from ion beam damage and correct for stage and/or specimen drift, i.e., perpendicular to the image face of the volume to be milled. Trenches on both sides of the region of interest were created to minimize re-deposition during automated milling and imaging. Imaging fiducials were generated for both ion and electron beam imaging and were used to dynamically correct for drift in the x- and y-directions by applying appropriate SEM beam shifts. Ion beam milling was performed at an accelerating voltage 30 kV and beam current of 9.3 nA, stage tilt of 9°, and working distance of 4 mm. With each milling step, 10 nm thickness of the material was removed. Each newly milled block face was imaged with the through-the-lens detector for backscattered electrons (TLD-BSE) at an accelerating voltage of 2 kV, beam current of 0.4 nA, stage tilt of 47°, and working distance of 3 mm. The pixel resolution was 10.3 nm with a dwell time of 30 μs. Pixel dimensions of the recorded image were 1536 × 1024 pixels. Seven hundred and forty-three images were collected and the contrast of the images inversed. Visualization and direct 3-D volume rendering of the acquired dataset was performed with Amira 6.0.1 (FEI Company, Hillsboro, OR USA).

MTEC and ependymal cell experiments—Mouse tracheal epithelia cell (MTEC) cultures were established as previously described (Mahjoub et al., 2010; You et al., 2002). Briefly, C57BL/6 mice were sacrificed at 2–4 months of age, trachea were excised, opened longitudinally to expose the lumen, and placed in 1.5 mg/mL Pronase E in DMEM/F12 medium (Life Technologies) at 4°C overnight. Tracheal epithelial cells were dislodged by gentle agitation and collected in DMEM/F12 with 10% FBS. After centrifugation, cells were treated with 0.5 mg/mL DNase I for 5 min on ice and centrifuged at 4°C for 10 min at 400 g. Cells were resuspended in DMEM/F12 with 10% FBS and plated in a tissue culture dish for 5 h at 37°C with 5% CO_2 to adhere contaminating fibroblasts. Non-adhered cells were then collected, concentrated by centrifugation, resuspended in an appropriate volume of mTEC-Plus medium (You et al., 2002), and seeded onto Transwell-Clear permeable filter supports (Corning).

To eliminate parental centrioles, cells were incubated in the presence of 1uM centrinone A (Nanjundappa et al., 2019) for 6 days. Air-liquid interface (ALI) was established 2 days after cells reached confluence by feeding mTEC-Serum-Free medium only in the lower chamber. Cells were cultured at 37°C with 5% CO_2, and media replaced every 2 days, and fixed on the indicated days. All chemicals were obtained from Sigma Aldrich unless otherwise indicated. Media were supplemented with 100 U/mL penicillin, 100 mg/mL streptomycin, and 0.25 mg/mL Fungizone (all obtained from Thermo Fisher).

For establishing directional flow in ALI mouse culture, tracheal progenitor cells were isolated and seeded onto 12 mm Transwell-Clear permeable filter supports as described above. To eliminate parental centrioles, cells were incubated in mTEC-Plus medium supplemented with 1uM centrinone A for up to 6–8 days. Air-liquid interface was

established two days after cells reached confluence by incubating cells in mTEC-Serum-Free, and centrinone was maintained in the medium throughout the differentiation process. A small volume (100uL) of mTEC-Serum-Free (with or without centrinone) was added to the upper chamber, and culture plates were placed on a nutating shaker (Fisher Scientific). Samples were rotated in a counter-clockwise direction at a speed of one rotation every 3 seconds, yielding an estimated directional flow rate of 12.5mm/sec. Cells were cultured at 37°C with 5% CO_2 with media replaced every two days. Cells were fixed and stained for centrioles and basal feet as described.

For ependymal cell culturing, all animal studies were performed in accordance with the guidelines of the European Community and French Ministry of Agriculture and were approved by the Ethic comity Charles Darwin (C2EA-05) and “Direction départementale de la protection des populations de Paris”, (Approval number Ce5/2012/107; APAFiS #9343). The mouse strain, Cen2-GFP (CB6-Tg(CAG-EGFP/CETN2)3–4Jgg/J, The Jackson Laboratory), has already been described by Higginbotham (Higginbotham et al., 2004). For *in vivo* analysis, animals used were homozygous for the Cen2-GFP. Lateral walls of the lateral brain ventricles were dissected as previously explained (Delgehyr et al., 2015). The tissue was treated with 0.1% triton in BRB80 (80 mM K-Pipes pH6.8; 1 mM MgCl2; 1 mM Na-EGTA) for 1 min prior to fixation and fixed in methanol at −20°C for 10 min. Saturation and antibody incubations were performed in PBS containing 10% FBS and 0.1% triton. Primary antibodies (CNTRL (monoclonal mouse from Santa Cruz) and CEP164) were incubated overnight (4°C). Secondary antibodies conjugated with Alexa Fluor −555 and −647 were incubated for 1h.

For *in vitro* pulse-chase experiments, cultures were performed as previously described. Transfection of ependymal cell progenitors was performed at 80% of confluency during the proliferation phase with a CMV-TagRFP-Cen1 plasmid (gift from Xavier Morin, ENS, Paris), which codes for human centrin 1 fused to TagRFP under the control of a CMV promoter, using jetPRIME Polyplus kit. Cells (in 25cm^3 flask) were transfected with a mix of 0.75µg of DNA, 300µL of jetPRIME Buffer and 1.5µL of jetPRIME transfection reagent in 3 mL of fresh complete medium (DMEM-Glutamax (Thermofisher) containing 10% FBS and 1% Penicillin/Streptomycin). After 4 hours at 37°C in 5% CO_2 incubator, the medium was renewed. One day after proliferation, cells were shaken at 250rpm overnight. Cells were plated on coverslips or Labtek chambers slides coated with L-Polylysin (40 µg/ml in pure water) at a density of 0.75×10^4 cells per µl in 20 or 60 µl drops. The medium was then replaced by serum-free DMEM-Glutamax-I 1% P/S, to trigger ependymal differentiation in vitro (DIV0). Cells were either fixed with Paraformaldehyde (4% in PBS) for 10min or used for live imaging between DIV3 and DIV6. Fixed cells were examined with an upright epifluorescence microscope (Zeiss Axio Observer.Z1) equipped with Apochromat X63 (NA 1.4) or X100 (NA 1.4) oil-immersion objectives and a Zeiss Apotome with an H/D grid. Fields of views with cells showing RFP-tagged centrosomal centrioles were acquired using Zen software with 230-nm z-steps and analyzed with image-J.

For live imaging, differentiating ependymal cells with two bright RFP-positive/EGFP positive centrosomal centrioles and RFP-negative/EGFP-positive procentrioles in amplification or growth-phases and filmed using an inverted spinning disk Nikon Ti PFS

microscope equipped with an oil-immersion X100 (NA 1.4) objective, an Evolve EMCCD Camera (Photometrics), dpss lasers (491 nm, 561 nm), a motorized scanning deck and an incubation chamber (37°C; 5% CO2; 80% humidity). Laser intensities and image capture times were respectively set to 20%, 50 ms for 488 nm and 25%, 100 ms for 561 nm. Images were acquired with Metamorph software at 60 minutes time interval for 24 hours. Image stacks were recorded with a z-distance of 0.7 mm. Four dimensional (x, y, z, t) time-lapse images were analyzed with Image J.

Semi-quantitative RT-PCR—RNA was purified from 1.5×10^5 cells on coverslips using the RNeasy Micro Kit (QIAGEN, 74000). Reverse transcription was performed using SuperScript III First-Strand Synthesis System for RT-PCR (Invitrogen, 18080–051). PCR was performed on cDNA using the primers 5'-AGAAGAACGGCATCAAGGTG-3' and 5'-GAACTCCAGCAGGACCATGT-3' for EGFP, 5'-AACACCGAGATGCTGTACCC-3' and 5'-ACGTAGGTCTCTTTGTCGGC-3' for tagRFP and 5'-ACCCCACCGTGTTCTTCGAC-3' and 5'-CATTTGCCATGGACAAGATG-3' for cyclophilin. Images of the gels were then analysed on ImageJ. The ratio between EGFP or tagRFP and cyclophilin band intensity were calculated. Quantifications of 3 independent experiments were pooled and plotted.

QUANTIFICATION AND STATISTICAL ANALYSIS

Positional analysis of hybrid cilium and basal body alignment assay—Custom written MATLAB script was used to determine the position of the hybrid cilia in multiciliated cells relative to cilia beating direction (can be accessed via the following link: https://drive.google.com/open?id=182KAccJf6YC69WbovKgTwtg62Y5DTadA). First, intensity thresholds for all channels were chosen for and binary images were generated to identify individual basal body and basal foot objects. Individual cells were outlined via manual cell border drawing. Basal body-basal foot pairs were identified based on the pairwise nearest neighbour search with a distance threshold of ~600 nm. The direction of a single cilium was defined as from the weighted center of the basal body object to that of the paired basal foot. All cilia directions in one cell were determined and the mean direction was regarded as the direction of beating in a cell. The cilia beating angles obtained were transformed into a two-dimensional unit vector: $r_i = \left(\frac{coscos\ a_i}{coscos\ a_i}\right)$. The resultant vector was the average of all the unit vectors in a cell: $\bar{r} = \frac{1}{n}\sum_{i=1}^{n} r_i$. The resultant vector length r was defined as the norm of the resultant vector: r = $\|\underline{r}\|$. The circular standard deviation was defined as: $= \sqrt{-2ln}(r)$. All the directions in a single cell were also subject to Rayleigh's test for uniformity distribution. The p-value is calculated as: $= e\left(\sqrt{\left(1 - 4n + 4n^2 - 4r_n^2\right) - (1 + 2n)}\right)$; $r_n = r \times n$. A p-value < 0.05 indicated that the cilia in the cell are significantly aligned. Aligned vector length was defined to describe the cilia alignment level in a cell with values ranging from 1 to 0, with 1 indicating 100% alignment and 0 indicating no alignment. The mean beating direction of all cilia were defined as the cilia beating direction. The hybrid cilia position relative to the cilia beating direction was measured using the same basal foot and basal body markers in cells whose size is normalized to [−0.5; 0.5] both along the cilia

beating direction (regarded as cell length) and the direction perpendicular to it (regarded as cell width).

For analysis of basal body alignment, centers of basal bodies were firstly identified manually. Basal body alignment index for a cell was then calculated using all the basal body coordinates as input by running an algorithm reported previously (Herawati et al., 2016). Briefly, a local basal body alignment index was calculated for each basal body within a cell and the basal body alignment index for a cell is the average of all local values within it. To calculate local basal body alignment index, the neighbouring basal bodies for the basal body were identified firstly by applying a distance threshold (1.3d, d represents the averaged nearest neighbour distance of basal bodies from 3 control images). Next, for i^{th} basal body with n neighbours, local index Ia, i was evaluated using a set of equations shown below. Ia,i value falls between 0 and 1 with 0 as no alignment and 1 as highly aligned.

$$\begin{cases} if\ n = 1,\ i = Ia, j\ if\ j\ has\ 2\ neighbours;\ Ia, i = 0\ if\ j\ has\ \leq 1\ or\ \geq 3\ neibours; \\ if\ n = 2\ or\ 3,\ Ia, i\ is\ calculate\ using\ equation\ 1, 2\ and\ 3\ below; \\ if\ n \geq 4\ or\ n = 0,\ Ia, i = 0. \end{cases}$$

$$Ia,\ i = \frac{\sum_{k>j}^{n} \sum_{j=1}^{n-1} \left[W_{jk} L\left(\phi_{jk}\right) \right]}{\sum_{k>j}^{n} \sum_{j=1}^{n-1} W_{jk}}; \quad \text{equation 1}$$

$$L\left(\phi_{jk}\right) = \max_{0 \leq \phi_{jk} \leq \pi}\left(-\cos\phi_{jk},\ 0\right); \quad \text{equation 2}$$

$$W_{jk} = w_j w_k; w_l = \min_{0 \leq |r_l - r_i| \leq 1.3d}\left[1 - \frac{\left(|r_l - r_i| - d\right)}{(1.3d - d)}, 1\right]; \quad \text{equation 3}$$

ϕ_{jk} is the acute angle of the two vectors $\left(\mathrm{r_j} - \mathrm{r_i}\right)$ and $\left(\mathrm{r_k} - \mathrm{r_i}\right)$

Basal body alignment level for control and centrinone treatment samples from 3 independent biological replicates was measured. Statistics were performed by student's *t* test.

Statistical Analysis—Data was analysed in Microsoft Excel and Prism software. Statistical tests, sample sizes and number of biological or technical replicates were specified in figure legends or method details. Differences were regarded as significant if $p < 0.05$, unless otherwise stated.

Supplementary Material

Refer to Web version on PubMed Central for supplementary material.

ACKNOWLEDGEMENT

This project is funded by CIHR program grant # 391917 to VM and SD; National Heart, Lung and Blood Institute (R01-HL128370) and the Children's Discovery Institute of Washington University and St. Louis Children's Hospital (CDI-CORE-2019-813) to MRM; Z.L. was supported by the SickKids Restracomp Fellowship. The authors acknowledge PCD patients and volunteers for providing nasal cells for this study, Julie Avolio for help with nasal cell scraping. Jia Zhou, Cindy Fang and Jasmine Kang assisted in data analysis. Douglas Holmyard (EM facility, The Hospital for Sick Children) prepared TEM and FIB-SEM samples and helped set up EM imaging. McGill EM facility contributed to FIB-SEM acquisition. We thank Profs Sudipto Roi's lab, Jeremy Reiter's lab and Nick Berbari's lab for experimental help. We thank Profs Bornens, Pelletier, Cheeseman, Kyung Lee, Elsasser, Avidor-Reiss laboratories for sharing antibodies and plasmids.

REFERENCES

Al Jord A, Lemaitre AI, Delgehyr N, Faucourt M, Spassky N, and Meunier A (2014). Centriole amplification by mother and daughter centrioles differs in multiciliated cells. Nature 516, 104–107. [PubMed: 25307055]

Boisvieux-Ulrich E, Laine MC, and Sandoz D (1985). The orientation of ciliary basal bodies in quail oviduct is related to the ciliary beating cycle commencement. Biol Cell 55, 147–150. [PubMed: 2937490]

Boon M, Wallmeier J, Ma L, Loges NT, Jaspers M, Olbrich H, Dougherty GW, Raidt J, Werner C, Amirav I, et al. (2014). MCIDAS mutations result in a mucociliary clearance disorder with reduced generation of multiple motile cilia. Nature communications 5, 4418.

Chong WM, Wang WJ, Lo CH, Chiu TY, Chang TJ, Liu YP, Tanos B, Mazo G, Tsou MB, Jane WN, et al. (2020). Super-resolution microscopy reveals coupling between mammalian centriole subdistal appendages and distal appendages. Elife 9.

Clare DK, Magescas J, Piolot T, Dumoux M, Vesque C, Pichard E, Dang T, Duvauchelle B, Poirier F, and Delacour D (2014). Basal foot MTOC organizes pillar MTs required for coordination of beating cilia. Nat Commun 5, 4888. [PubMed: 25215410]

Clement CA, Ajbro KD, Koefoed K, Vestergaard ML, Veland IR, Henriques de Jesus MP, Pedersen LB, Benmerah A, Andersen CY, Larsen LA, et al. (2013). TGF-beta signaling is associated with endocytosis at the pocket region of the primary cilium. Cell Rep 3, 1806–1814. [PubMed: 23746451]

Delgehyr N, Meunier A, Faucourt M, Bosch Grau M, Strehl L, Janke C, and Spassky N (2015). Ependymal cell differentiation, from monociliated to multiciliated cells. Methods Cell Biol 127, 19–35. [PubMed: 25837384]

Frisch D, and Farbman AI (1968). Development of order during ciliogenesis. Anat Rec 162, 221–232. [PubMed: 5726142]

Frommer A, Hjeij R, Loges NT, Edelbusch C, Jahnke C, Raidt J, Werner C, Wallmeier J, Grosse-Onnebrink J, Olbrich H, et al. (2015). Immunofluorescence Analysis and Diagnosis of Primary Ciliary Dyskinesia with Radial Spoke Defects. Am J Respir Cell Mol Biol 53, 563–573. [PubMed: 25789548]

Funk MC, Bera AN, Menchen T, Kuales G, Thriene K, Lienkamp SS, Dengjel J, Omran H, Frank M, and Arnold SJ (2015). Cyclin O (Ccno) functions during deuterosome-mediated centriole amplification of multiciliated cells. EMBO J 34, 1078–1089. [PubMed: 25712475]

Galati DF, Mitchell BJ, and Pearson CG (2016). Subdistal Appendages Stabilize the Ups and Downs of Ciliary Life. Dev Cell 39, 387–389. [PubMed: 27875681]

Gibbons IR (1961). The relationship between the fine structure and direction of beat in gill cilia of a lamellibranch mollusc. J Biophys Biochem Cytol 11, 179–205. [PubMed: 13898346]

Gomperts BN, Gong-Cooper X, and Hackett BP (2004). Foxj1 regulates basal body anchoring to the cytoskeleton of ciliated pulmonary epithelial cells. J Cell Sci 117, 1329–1337. [PubMed: 14996907]

Guirao B, Meunier A, Mortaud S, Aguilar A, Corsi JM, Strehl L, Hirota Y, Desoeuvre A, Boutin C, Han YG, et al. (2010). Coupling between hydrodynamic forces and planar cell polarity orients mammalian motile cilia. Nat Cell Biol 12, 341–350. [PubMed: 20305650]

Herawati E, Taniguchi D, Kanoh H, Tateishi K, Ishihara S, and Tsukita S (2016). Multiciliated cell basal bodies align in stereotypical patterns coordinated by the apical cytoskeleton. J Cell Biol 214, 571–586. [PubMed: 27573463]

Higginbotham H, Bielas S, Tanaka T, and Gleeson JG (2004). Transgenic mouse line with green-fluorescent protein-labeled Centrin 2 allows visualization of the centrosome in living cells. Transgenic Res 13, 155–164. [PubMed: 15198203]

Jain R, Pan J, Driscoll JA, Wisner JW, Huang T, Gunsten SP, You Y, and Brody SL (2010). Temporal relationship between primary and motile ciliogenesis in airway epithelial cells. Am J Respir Cell Mol Biol 43, 731–739. [PubMed: 20118219]

Kizilyaprak C, Stierhof YD, and Humbel BM (2019). Volume microscopy in biology: FIB-SEM tomography. Tissue Cell 57, 123–128. [PubMed: 30385054]

Knowles MR, Leigh MW, Carson JL, Davis SD, Dell SD, Ferkol TW, Olivier KN, Sagel SD, Rosenfeld M, Burns KA, et al. (2012). Mutations of DNAH11 in patients with primary ciliary dyskinesia with normal ciliary ultrastructure. Thorax 67, 433–441. [PubMed: 22184204]

Kunimoto K, Yamazaki Y, Nishida T, Shinohara K, Ishikawa H, Hasegawa T, Okanoue T, Hamada H, Noda T, Tamura A, et al. (2012). Coordinated ciliary beating requires Odf2-mediated polarization of basal bodies via basal feet. Cell 148, 189–200. [PubMed: 22265411]

Liu Z, Nguyen QPH, Guan Q, Albulescu A, Erdman L, Mahdaviyeh Y, Kang J, Ouyang H, Hegele RG, Moraes T, et al. (2020). A quantitative super-resolution imaging toolbox for diagnosis of motile ciliopathies. Sci Transl Med 12.

Lu CJ, Du H, Wu J, Jansen DA, Jordan KL, Xu N, Sieck GC, and Qian Q (2008). Non-random distribution and sensory functions of primary cilia in vascular smooth muscle cells. Kidney Blood Press Res 31, 171–184. [PubMed: 18483460]

Lu H, Anujan P, Zhou F, Zhang Y, Chong YL, Bingle CD, and Roy S (2019). Mcidas mutant mice reveal a two-step process for the specification and differentiation of multiciliated cells in mammals. Development 146.

Lucas JS, Davis SD, Omran H, and Shoemark A (2020). Primary ciliary dyskinesia in the genomics age. Lancet Respir Med 8, 202–216. [PubMed: 31624012]

Mahjoub MR, Xie Z, and Stearns T (2010). Cep120 is asymmetrically localized to the daughter centriole and is essential for centriole assembly. J Cell Biol 191, 331–346. [PubMed: 20956381]

Marshall WF, and Kintner C (2008). Cilia orientation and the fluid mechanics of development. Curr Opin Cell Biol 20, 48–52. [PubMed: 18194854]

Mazo G, Soplop N, Wang WJ, Uryu K, and Tsou MF (2016). Spatial Control of Primary Ciliogenesis by Subdistal Appendages Alters Sensation-Associated Properties of Cilia. Dev Cell 39, 424–437. [PubMed: 27818179]

McAuley JR, and Anand VK (1998). Clinical significance of compound cilia. Otolaryngol Head Neck Surg 118, 685–687. [PubMed: 9591872]

Mirzadeh Z, Han YG, Soriano-Navarro M, Garcia-Verdugo JM, and Alvarez-Buylla A (2010). Cilia organize ependymal planar polarity. J Neurosci 30, 2600–2610. [PubMed: 20164345]

Mitchell B, Jacobs R, Li J, Chien S, and Kintner C (2007). A positive feedback mechanism governs the polarity and motion of motile cilia. Nature 447, 97–101. [PubMed: 17450123]

Mitchell B, Stubbs JL, Huisman F, Taborek P, Yu C, and Kintner C (2009). The PCP pathway instructs the planar orientation of ciliated cells in the Xenopus larval skin. Curr Biol 19, 924–929. [PubMed: 19427216]

Monnich M, Borgeskov L, Breslin L, Jakobsen L, Rogowski M, Doganli C, Schroder JM, Mogensen JB, Blinkenkjaer L, Harder LM, et al. (2018). CEP128 Localizes to the Subdistal Appendages of the Mother Centriole and Regulates TGF-beta/BMP Signaling at the Primary Cilium. Cell Rep 22, 2584–2592. [PubMed: 29514088]

Nanjundappa R, Kong D, Shim K, Stearns T, Brody SL, Loncarek J, and Mahjoub MR (2019). Regulation of cilia abundance in multiciliated cells. Elife 8.

Olbrich H, Cremers C, Loges NT, Werner C, Nielsen KG, Marthin JK, Philipsen M, Wallmeier J, Pennekamp P, Menchen T, et al. (2015). Loss-of-Function GAS8 Mutations Cause Primary Ciliary Dyskinesia and Disrupt the Nexin-Dynein Regulatory Complex. American journal of human genetics 97, 546–554. [PubMed: 26387594]

Omran H, Haffner K, Volkel A, Kuehr J, Ketelsen UP, Ross UH, Konietzko N, Wienker T, Brandis M, and Hildebrandt F (2000). Homozygosity mapping of a gene locus for primary ciliary dyskinesia on chromosome 5p and identification of the heavy dynein chain DNAH5 as a candidate gene. Am J Respir Cell Mol Biol 23, 696–702. [PubMed: 11062149]

Paintrand M, Moudjou M, Delacroix H, and Bornens M (1992). Centrosome organization and centriole architecture: their sensitivity to divalent cations. J Struct Biol 108, 107–128. [PubMed: 1486002]

Reiter JF, and Leroux MR (2017). Genes and molecular pathways underpinning ciliopathies. Nat Rev Mol Cell Biol 18, 533–547. [PubMed: 28698599]

Spassky N, and Meunier A (2017). The development and functions of multiciliated epithelia. Nat Rev Mol Cell Biol 18, 423–436. [PubMed: 28400610]

Stubbs JL, Oishi I, Izpisua Belmonte JC, and Kintner C (2008). The forkhead protein Foxj1 specifies node-like cilia in Xenopus and zebrafish embryos. Nat Genet 40, 1454–1460. [PubMed: 19011629]

Stubbs JL, Vladar EK, Axelrod JD, and Kintner C (2012). Multicilin promotes centriole assembly and ciliogenesis during multiciliate cell differentiation. Nat Cell Biol 14, 140–147. [PubMed: 22231168]

Uzbekov R, and Alieva I (2018). Who are you, subdistal appendages of centriole? Open Biol 8.

Vladar EK, Bayly RD, Sangoram AM, Scott MP, and Axelrod JD (2012). Microtubules enable the planar cell polarity of airway cilia. Curr Biol 22, 2203–2212. [PubMed: 23122850]

Vladar EK, and Stearns T (2007). Molecular characterization of centriole assembly in ciliated epithelial cells. J Cell Biol 178, 31–42. [PubMed: 17606865]

Wallmeier J, Al-Mutairi DA, Chen CT, Loges NT, Pennekamp P, Menchen T, Ma L, Shamseldin HE, Olbrich H, Dougherty GW, et al. (2014). Mutations in CCNO result in congenital mucociliary clearance disorder with reduced generation of multiple motile cilia. Nature genetics 46, 646–651. [PubMed: 24747639]

Wallmeier J, Frank D, Shoemark A, Nothe-Menchen T, Cindric S, Olbrich H, Loges NT, Aprea I, Dougherty GW, Pennekamp P, et al. (2019). De Novo Mutations in FOXJ1 Result in a Motile Ciliopathy with Hydrocephalus and Randomization of Left/Right Body Asymmetry. American journal of human genetics 105, 1030–1039. [PubMed: 31630787]

Wong YL, Anzola JV, Davis RL, Yoon M, Motamedi A, Kroll A, Seo CP, Hsia JE, Kim SK, Mitchell JW, et al. (2015). Cell biology. Reversible centriole depletion with an inhibitor of Polo-like kinase 4. Science 348, 1155–1160. [PubMed: 25931445]

Wu J, Du H, Wang X, Mei C, Sieck GC, and Qian Q (2009). Characterization of primary cilia in human airway smooth muscle cells. Chest 136, 561–570. [PubMed: 19318679]

You Y, Richer EJ, Huang T, and Brody SL (2002). Growth and differentiation of mouse tracheal epithelial cells: selection of a proliferative population. Am J Physiol Lung Cell Mol Physiol 283, L1315–1321. [PubMed: 12388377]

Zhao H, Zhu L, Zhu Y, Cao J, Li S, Huang Q, Xu T, Huang X, Yan X, and Zhu X (2013). The Cep63 paralogue Deup1 enables massive de novo centriole biogenesis for vertebrate multiciliogenesis. Nat Cell Biol 15, 1434–1444. [PubMed: 24240477]

Highlights:

- Multiciliated cells contain a hybrid cilium with features of primary and motile cilium
- The hybrid cilium originates from parental centriole
- The hybrid cilium position is biased towards the cilia beating direction
- The hybrid cilium functions in basal body alignment

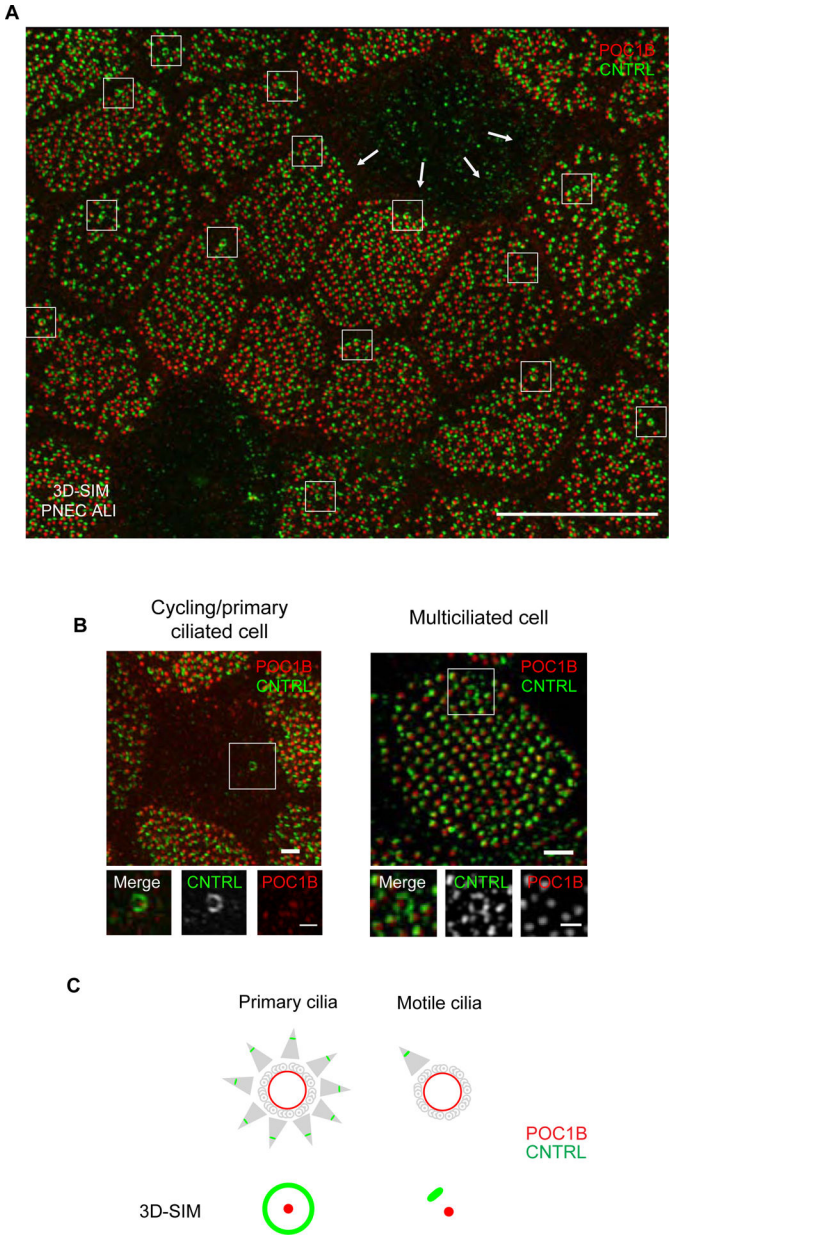

Figure 1. Super-resolution reveals a basal body with multiple basal feet in airway multiciliated cells

(A) 3D-SIM volume maximum intensity projection of large field of view of nasal primary airway multiciliated cell (PNEC) grown in air liquid interphase labeled with anti-CNTRL (green) and anti-POC1B (red) antibodies. Note the ring-like pattern of CNTRL localization encircling the basal body labeled by POC1B (boxed areas). Scale bar represents 10 μm. ALI, air liquid interface. (B) 3D-SIM volume maximum intensity projection of an airway cycling/primary ciliated cell (left) or nasal airway multiciliated cell (right) grown in ALI labeled with anti-CNTRL (green) and anti-POC1B (red) antibodies. Scale bars represent 1 μm and 500 nm (boxed areas). (C) Cartoon representation of basal body-basal foot structure by TEM in cells with primary or motile cilia (upper panel) and by 2 colour 3D-SIM imaging of basal body and basal foot (lower panel). By 3D-SIM microscopy the basal body protein POC1B

appears as a dot while the basal foot protein CNTRL appears as a dot in motile cilia, but as a ring in primary cilia. Red represents localization of POC1B and green represents localization of CNTRL. See also Figure S1.

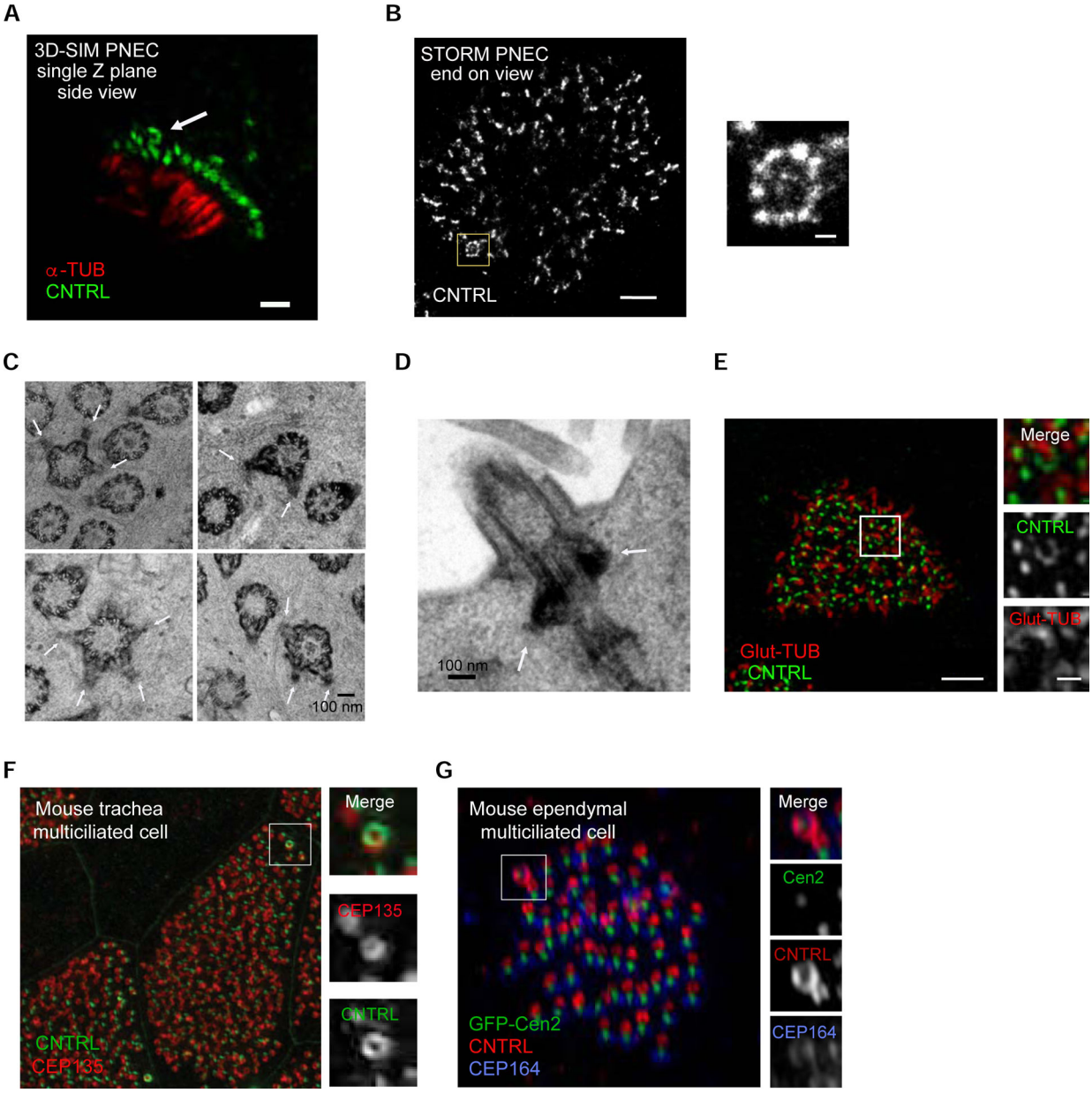

Figure 2. The basal body extrudes a cilium and is conserved in different mammalian primary cells, tissues and species.

(A) 3D-SIM single-plane image of a human nasal airway multiciliated cell freshly isolated from a healthy individual, labeled with anti-CNTRL (green) and anti-alpha-tubulin (red) antibodies, showing the presence of the basal body with multiple basal feet. Scale bar represents 1 μm. (B) Left: STORM micrograph of airway multiciliated cell labeled with anti-CNTRL antibody, showing a distinct ring-like distribution of CNTRL (boxed area). Right: High-magnification view of boxed area. Scale bars represent 1 μm (left) and 100 nm (right). (C) Collage of representative TEM micrographs showing basal bodies harbouring multiple basal feet in ALI-cultured human airway multiciliated cells (see white arrows). Scale bar represents 100 nm. (D) TEM micrograph showing axoneme emanating from basal bodies harbouring multiple basal feet (in white arrows) in human airway multiciliated cell. Scale

bar represents 1 μm. (E) Left: 3DSIM volume maximum intensity projection of an ALI-cultured human airway multiciliated cell labeled with anti-CNTRL (green) and anti-Glut-TUB (red) antibodies. Note the axoneme emanating from ring-like structure labeled with CNTRL (boxed area). Right: High-magnification view of boxed area with individual channels. Scale bars represent 2 μm (left) and 500 nm (right). (F) 3D-SIM volume maximum intensity projection of mouse tracheal multiciliated cell (ALI D20), labeled with anti-CNTRL (green) and anti-CEP135 (red) antibodies. Right: High-magnification view of boxed area with individual channels. Scale bar represents 2 μm. (G) 3D-SIM volume maximum intensity projection of adult mouse ependymal multiciliated cells (P16), labeled with GFP-Centrin2 (basal body), anti-CNTRL (red) and anti-CEP164 (blue, distal appendage protein) antibodies. Right: High-magnification view of boxed area labeled in left. Scale bar represents 1 μm and 200 nm.

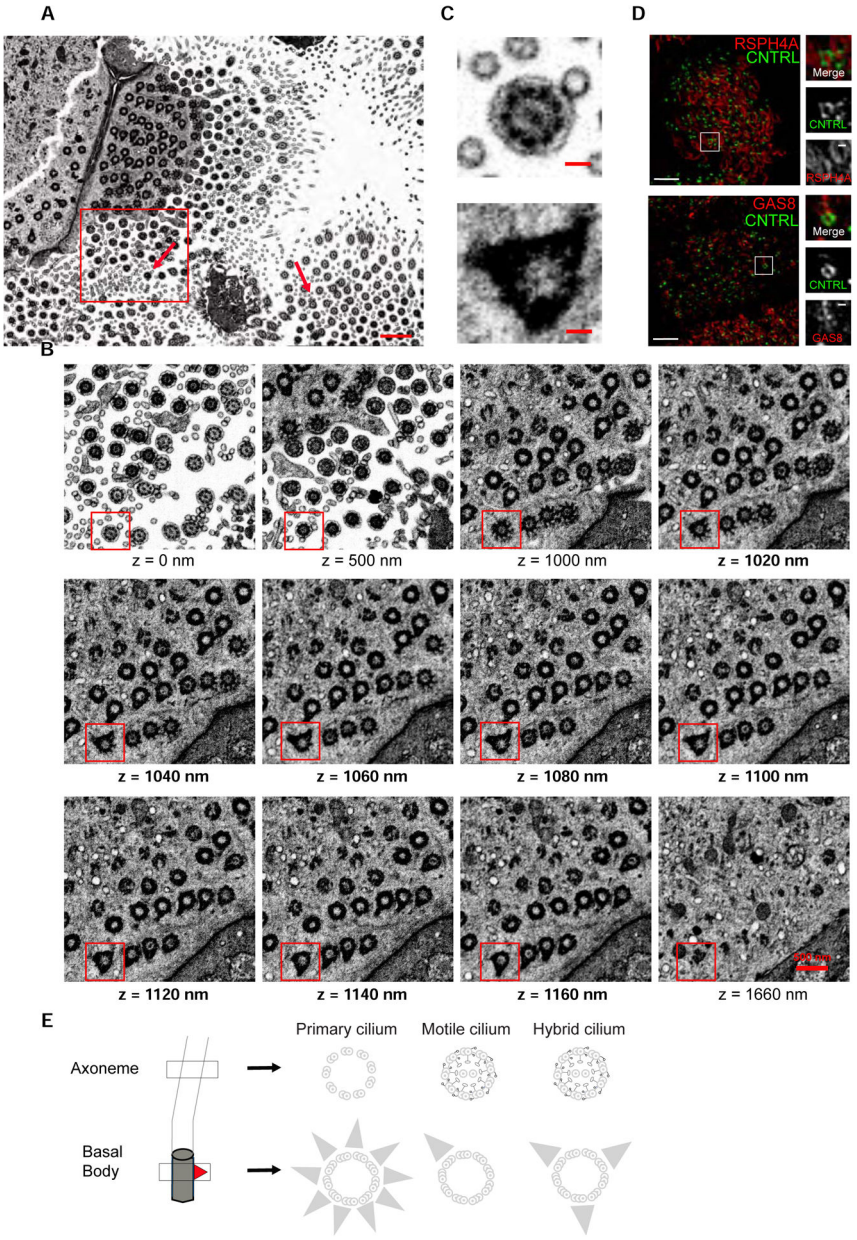

Figure 3. The cilium has hybrid features between primary and motile cilia

(A) Representative section from FIB-SEM tomogram of human primary nasal multiciliated cells. Arrows indicate basal bodies with multiple basal feet. Scale bar represents 1 μm. (B) High-magnification view of boxed area in (A) at different z positions of the tomogram from z=0 nm to z=1660 nm. Note the hybrid cilium axoneme and central pair (z=0 nm), transition fibers (z=1000–1040 nm), multiple basal feet (z=1160–1160 nm) and the absence of the endocytic pocket (z=1660 nm). Scale bar represents 500 nm. (C) A high-magnification view of boxed area in (B) highlighting the basal body with a central pair and multiple basal feet. Scale bar represents 100 nm. (D) 2D projection micrographs of 3D-SIM volume of human airway multiciliated cells (left), and high-magnification views of boxed areas (right), labeled with anti-CNTRL (green), anti-RSPH4A (red, top) and anti-GAS8 (red, bottom) antibodies.

Scale bars represent 2 μm. (E) Cartoon representation of hybrid cilium structure relative to the primary cilium and motile cilium. The axoneme extends from the basal body (grey), each with a basal foot (red triangle). The basal body of the primary cilium presents multiple basal feet, while the one of the motile cilium has one basal foot. In regard to the axoneme, the motile cilium presents outer dynein arms, inner dynein arms, nexin-dynein regulatory complexes, radial spokes and central pair complexes (black) , which are critical for in plane ciliary beating. The hybrid cilium has features of both the primary and motile cilium, namely multiple basal feet and protein complexes critical for ciliary beating.

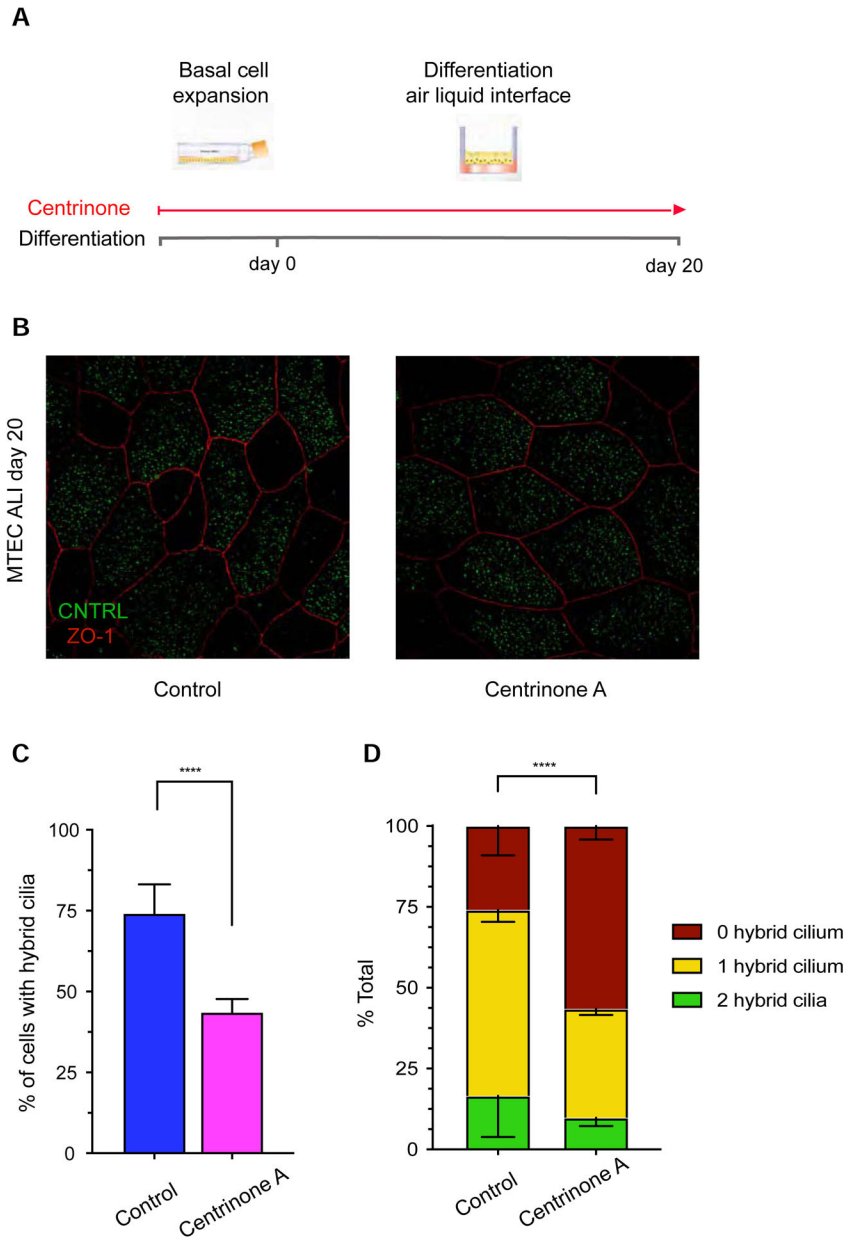

Figure 4. Hybrid cilium originates from parental centrioles

(A) Cartoon representation of centrinone A treatment in mouse tracheal multiciliated cells. (B) 2D projection micrograph of 3D-SIM volume of representative example of mouse tracheal multiciliated cells at ALI D20 treated with DMSO control or centrinone A labeled with anti-CNTRL (green) and anti-ZO-1 (red) antibodies. Arrowheads indicate CNTRL rings. Scale bar represents 5 μm. (C) Bar graphs representing percentage of cells with hybrid cilium in DMSO control (blue) and centrinone A-treated (pink) cells treated during basal cell expansion and throughout differentiation; n>800 over three independent biological replicates. Data are represented as mean ± SD. Statistical analysis was done using Cochran-Mantel-Haenszel test. **** $p<0.0001$. (D) Bar graph representing percentage of cells with none (red), one (yellow) or two (green) hybrid cilia in ALI D20 mouse tracheal multiciliated

cells treated with DMSO control (left) or centrinone A (right); n>800 over three independent biological replicates. Data are represented as mean ± SD. Statistical analysis was done using Chi-square test. See also Figures S2 and S3.

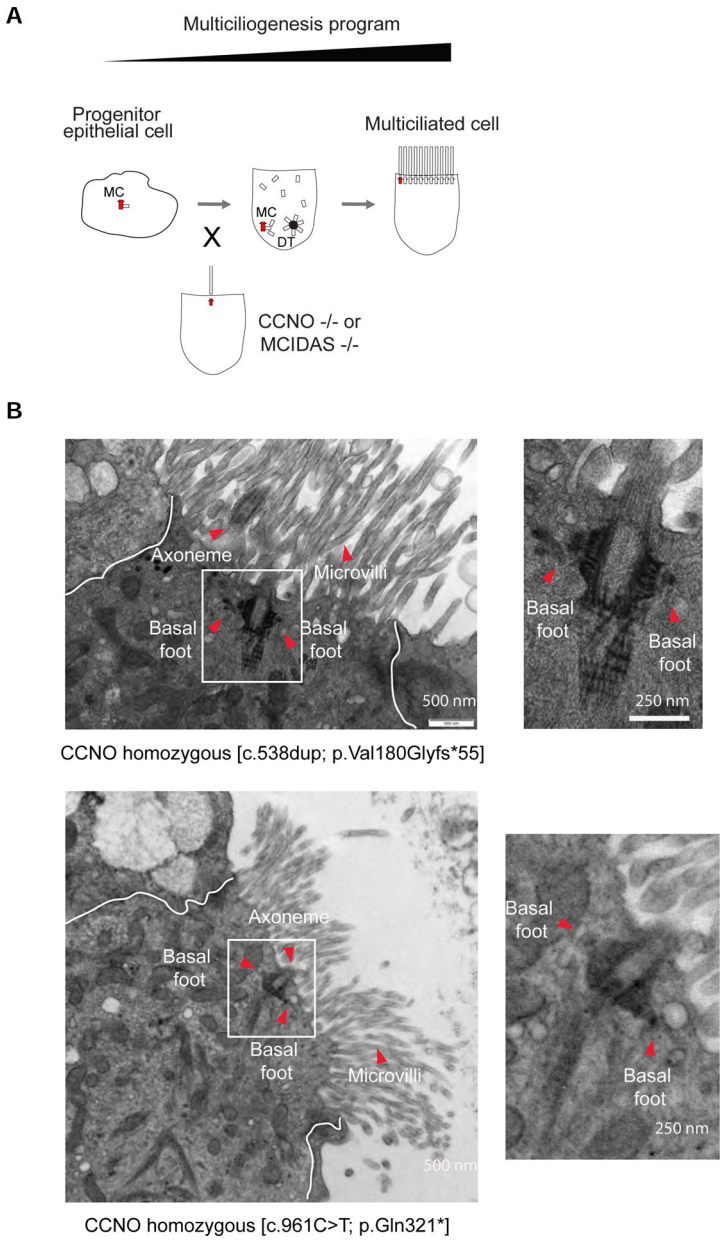

Figure 5. Hybrid cilium formation is independent from other motile cilia in airway multiciliated cells

(A) Cartoon depicting a simplified version of the multiciliogenesis cellular program. Note CCNO and MCIDAS loss of function mutations lead to oligocilia phenotype. MC, mother centriole. DT, deuterostome. (B) Left: TEM micrographs of a human airway multiciliated cells isolated from nasal epithelium of PCD patients with CCNO loss of function early termination mutations. Boxed areas represent basal bodies with multiple basal feet. Red arrowheads indicate axoneme, basal feet and microvilli. Right: High-magnification views of boxed area. Scale bars represent 500 nm (left) and 250 nm (right).

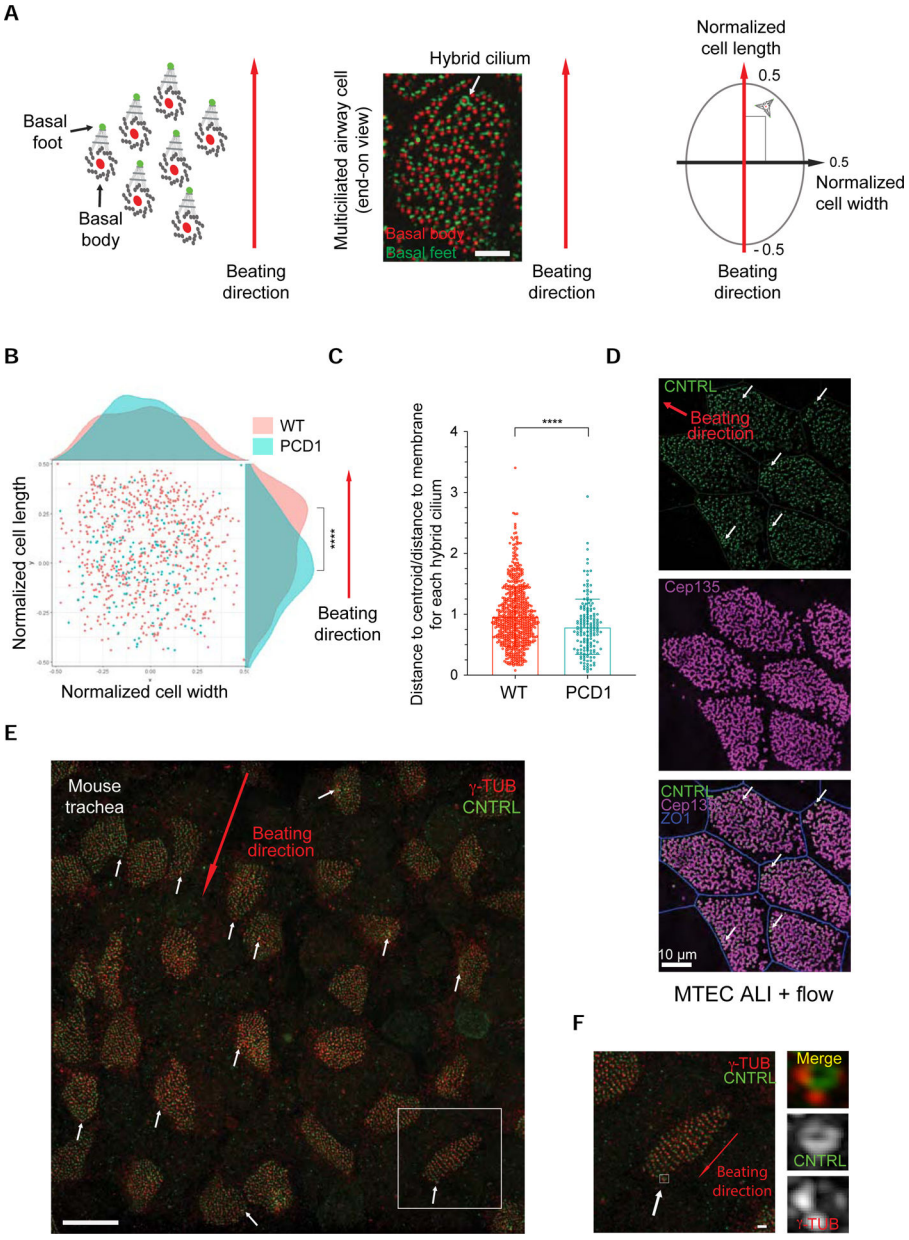

Figure 6. Hybrid cilium position is biased in the direction of beating and dependent on flow

(A) Left: Cartoon depiction of the strategy for analysis of the position of the hybrid cilium relative to cilia beating direction. Middle: representative 3DSIM image used for data analysis. Scale bar represents 5μm. Right: MATLAB-based analysis strategy to assess rotational polarity in multiciliated cells. The position is calculated relative to coordinates (−0.5<x,y<+0.5) obtained by normalizing the cell length and width to 1. Cell length (y-axis) is assigned as parallel to the direction of ciliary beating measured by rotational polarity of basal bodies-basal feet pairs, cell width (x-axis) is assigned as perpendicular to the direction of ciliary beating. (B) Scatterplot showing the cumulative distribution of hybrid cilia along normalized cell width and cell length in human airway multiciliated cells from three healthy individuals (red) or one PCD patient with immotile cilia (green) caused by loss-of-function

mutations in DNAH5 (p.[(Arg478*) and intronic mutation abolishing accepted splice-site for exon 68]), indicating a positional bias toward the direction of ciliary beating (See also two other PCD patients in Figure S8). Each dot represents a hybrid cilium in a cell; Healthy n=694, PCD1 =165, **** p<0.0001, student's t-test. (C) Scatterplot-bar graphs showing distribution of ratio of hybrid cilium-cell centroid distance to hybrid cilium-cell membrane shortest distance of human airway multiciliated cells from healthy individuals or PCD1 patient. Each dot represents a hybrid cilium in a cell; Healthy n=694, PCD n=277, p<0.0001, student's t-test. **** p<0.0001. Data are represented as mean ± SD. (D) 3D-SIM volume maximum intensity projection of MTEC labeled with anti-CNTRL (green) antibody, anti-CEP135 (magenta) and anti-ZO1 (blue) subjected to rotational movement to facilitate flow generation in transwells. Arrows indicate CNTRL rings. MTEC ALI, mouse trachea epithelia cells growing at air liquid interface. (E) 3D-SIM volume maximum intensity projection of mouse tracheal tissues labelled with anti-CNTRL (green) antibody and anti-γTub (red). Arrow indicates beating direction. Scale bar represents 10 μm. (F) High-magnification view of boxed area in (E). Note hybrid cilium basal body presenting multiple basal feet harbouring γ-Tubulin labeling. Scale bar represents 1 μm. See also Figure S4.

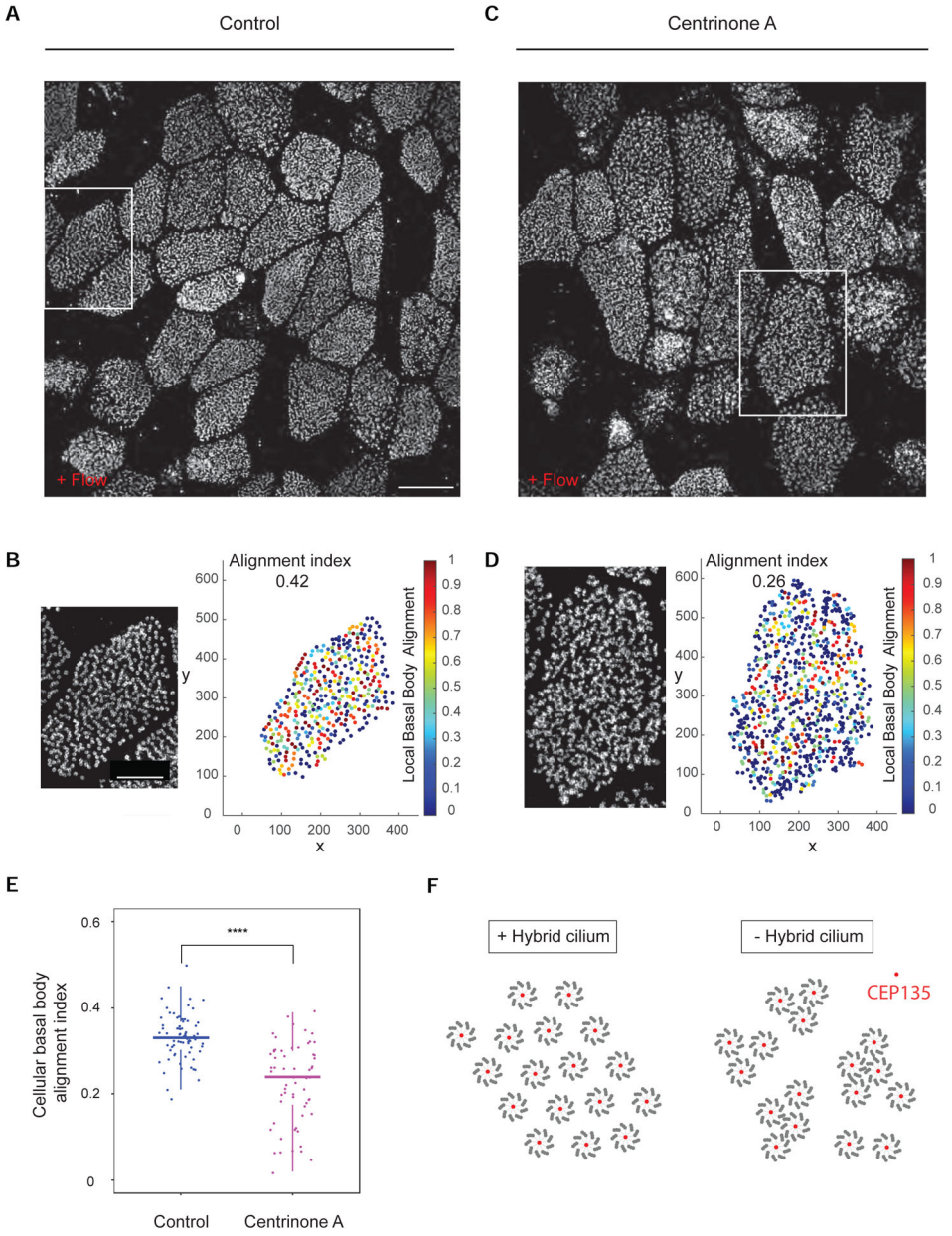

Figure 7. Hybrid cilium is critical for establishing basal body alignment

(A) 3D-SIM volume maximum intensity projection of mouse tracheal multiciliated cell (ALI D20), treated with DMSO (control) from basal cells expansion throughout ALI differentiation labeled with anti-CEP135 antibodies. Scale bar represents 10 μm. (B) Left: High-magnification view of boxed area in (A). Right: relative basal body local and global alignment measurements. (C) 3D-SIM volume maximum intensity projection of mouse tracheal multiciliated cell (ALI D20), treated centrinone A (right) from basal cells expansion throughout ALI differentiation labeled with anti-CEP135 antibodies. Scale bar represents 10 μm. (D) Left: High-magnification view of boxed area in (C). Right: relative basal body local and global alignment measurements. (E) Quantification of cellular basal body alignment index in cells treated with DMSO or centrinone A throughout multiciliated cells

differentiation (n=70 over 3 independent biological replicates, total 63 cells. DMSO=0.33±0.05; centrinone A=0.23±0.09). Statistical analysis was done using unpaired t-test. Data are represented as mean ± SD. **** $p<0.0001$. (F) A model showing function of the hybrid cilia. When hybrid cilium is present, basal bodies are well aligned. However, when hybrid cilium is removed by centrinone A, basal body alignment in the cell is disrupted and basal bodies tend to group into clusters. Red present basal body protein CEP135, surrounded by 9 axonemal microtubule triplets.

KEY RESOURCES TABLE

REAGENT or RESOURCE	SOURCE	IDENTIFIER
Antibodies		
Rabbit anti-CEP128	Abcam	Ab11879
Rabbit anti-ODF2	Abcam	Ab43840
Rabbit anti-ODF2	Gift from Kyung Lee lab at NIH	N/A
Rabbit anti-CNTRL	Santa Cruz	Sc-135020
Mouse anti-CNTRL	Atlas Antibodies	HPA020468
Rabbit anti-CNTRL	Santa Cruz	Sc-365521
Rabbit anti-CNTRL	Atlas Antibodies	HPA051583
Rabbit anti-POC1B	Invitrogen	PA5–24495
Rat anti-POC1B	Gift from Tomer Avidor-Reiss lab at University of Toledo	N/A
Mouse anti-polyglutamylation modification	Adipogen	AG-20B-0020-C1(GT355)
Mouse anti-TUBA4A(a-tubulin)	Sigma-Aldrich	T9026(DM1A)
Mouse anti-TUBA4A(a-tubulin-FITC conjugated)	Sigma-Aldrich	F2168(DM1A)
Mouse anti-g-tubulin	Sigma-Aldrich	T6557
Rabbit anti-RSPH4A	Atlas Antibodies	HPA031196
Rabbit anti-GAS8	Atlas Antibodies	HPA041311
Mouse anti-acetylated a-tubulin	Sigma-Aldrich	T7451
Rat anti-ZO-1	Gift from Moe Mahjoub lab at Washington University	N/A
Rabbit-Arl13B	Gift from William Trimble Lab at the Hospital for Sick Children	
Goat anti rabbit IgG Alex fluor 488	Thermo Fisher	A11034
Goat anti mouse IgG Alex fluor555	Thermo Fisher	A21424
Goat anti rabbit IgG Alexa fluor 405	Thermo Fisher	A-31556
Goat anti rabbit F(ab')2 Alexa fluor 647	Thermo Fisher	A21246
HRP-conjugated anti-IgG antibodies	Cell Signaling	7074, 7076
Biological Samples		
Mouse tracheal epithelia cells	This study	N/A
Mouse ependymal epithelia cells	This study	N/A
Human airway multiciliated cells from patient PCD1(DNAH5: allele1: intronic, abolishes accepted splice site for exon68, allele2:p.Arg478*)	This study	N/A
Human airway multiciliated cells from patient PCD2 (DNAH11: allele1: pCys4286*, allele2:pIle4122Ser)	This study	N/A
Human airway multiciliate cells from patient PCD3(DNAH5, homogenous, pPhe634fs*2)	This study	N/A
Chemicals, Peptides, and Recombinant Proteins		

REAGENT or RESOURCE	SOURCE	IDENTIFIER
DMEM/F-12	Thermofisher	11320033
PneumaCult-Ex medium	Stem Cell Technologies	5008
PneumaCult-ALI medium	Stem Cell Technologies	05001
Paraformaldehyde	Electron Microscopy Sciences	15710
Centrinone A	from Moe Mahjoub lab at Washington University	N/A
RIPA lysis buffer	Pierce, Thermo Fisher Scientific	89900
Critical Commercial Assays		
APEX Antibody labeling kit	Thermo Fisher Scientific	A10470, A10468
Novex ECL Chemiluminescent Substrate Kit	Invitrogen	WP20005
RNeasy Micro Kit	QIAGEN	7400
SuperScript III First-Strand Synthesis System for RT-PCR	Invitrogen	18080–051
Gibson Assemby Kit	New England Biolabs	E2611S
Experimental Models: Organisms/Strains		
Mouse strain: CEN2-GFP	The Jackson Laboratory; Higginbotham et al., 2004	CB6-Tg(CAG-EGFP/CETN2)3–4Jgg/J
Oligonucleotides		
Primers for EGFP semi quantitiative RT-PCR: FOR: AGAAGAACGGCATCAAGGTG;	This study	N/A
Primers for EGFP semi quantitiative RT-PCR: REV: GAACTCCAGCAGGACCATGT’	This study	N/A
Primers for tagRFP semi quantitiative RT-PCR: FOR: AACACCGAGATGCTGTACCC;	This study	N/A
Primers for tagRFP semi quantitiative RT-PCR: REV: ACGTAGGTCTCTTTGTCGGC	This study	N/A
Primers for Cyclophilin semi quantitiative RT-PCR: FOR: ACCCCACCGTGTTCTTCGAC;	This study	N/A
Primers for Cyclophilin semi quantitiative RT-PCR: REV: CATTTGCCATGGACAAGATG	This study	N/A
Recombinant DNA		
CMV-TagRFP-Cen1 plasmid	Gift from Xavier Morin lab at CNRS	N/A
Software and Algorithms		
FIJI-ImageJ	Schneider et al., 2012	https://imagej.net/Fiji
MATLAB	MathWorks	Version 2019b https://www.mathworks.com/products/get-matlab.html
ELYRA PS.1	Carl Zeiss Microscopy	Version PS.1
ZEN Black	Carl Zeiss Microscopy	Version 8.1
Excel	Microsoft	Version 2013
Prism	GraphPad	Version 8 https://www.graphpad.com/scientific-software/prism/
STORM image drift correction and binning	This study	https://drive.google.com/open?id=11fuWn7kmZ-loCn79CKChJI5FeMme0fDU

REAGENT or RESOURCE	SOURCE	IDENTIFIER
Auto Slice & View G3	FEI Company, Hillsboro, OR USA	https://www.fei.com/document/introducing-auto-slice-and-view-G3/#gsc.tab=0
Amira	FEI Company, Hillsboro, OR USA	6.0.1
Metamorph	Molecular Devices	N/A
Hybrid cilia position analysis	This study	https://drive.google.com/open?id=182KAccJf6YC69WbovKgTwtg62Y5DTadA
Basal body alignment analysis	This study	https://drive.google.com/open?id=182KAccJf6YC69WbovKgTwtg62Y5DTadA